AN ABSTRACT OF THE DISSERTATION OF

Michael C. Rowe for the degree of Doctor of Philosophy in Geology presented on April 27, 2006.

Title: The Role of Subduction Fluids in Generating Compositionally Diverse Basalts in the Cascadia Subduction Zone.

Abstract approved:

_____

Roger L. Nielsen, Adam J.R. Kent

The primary goal of this study is to assess the impact of a subduction component added to the mantle wedge beneath the Oregon Cascades to the composition and fO_2 of primitive Cascade basalts. Olivine-hosted melt inclusions from compositionally diverse basalts across the Cascade arc (~100 km) are utilized in an effort to reduce effects of assimilation and crystallization while retaining volatile phases lost during shallow degassing.

Many melt inclusions from Cascade samples require rehomogenization to melt daughter crystals formed from slow cooling of the basalts after inclusion entrapment. Rehomogenization of crystalline inclusions documents post-entrapment modification of inclusions from alkali-rich forearc lavas resulting in anomalously high FeO* (up to 21 wt%) from the dissolution of magnetite during rehomogenization.

Oxidation state in melt inclusions can be determined from electron microprobe measurements of sulfur speciation, based on the sulfur Kα peak shift. This technique in melt inclusions is largely unexplored and a series of experiments were conducted to determine the extent to which both natural processes and rehomogenization influence measured sulfur speciation. These experiments indicate that degassing (oxidation or reduction) and H^+ diffusion (oxidation) are the two most significant factors altering the sulfur speciation, however, Fe-loss and crystallization will also increase fO_2. Rehomogenization has relatively minor impact on sulfur speciation provided heating times are kept short (<10 minutes) and significant over- or under-heating has not occurred.

Oxygen fugacity, chlorine, and incompatible trace elements in primitive melt inclusions in Oregon Cascade basalts increase towards the trench, suggesting that the subarc mantle is oxidized as a result of addition of a subduction component. The overall fO_2 range of Cascade basalts, <-0.25 log units (ΔFMQ) to +1.9 log units (ΔFMQ), is consistent with previous results and is believed to be representative of the fO_2 range of the subarc mantle. Calc-alkaline basalts however appear to have re-equilibrated to lower fO_2 prior to inclusion entrapment.

A second goal of this study was to analyze phenocrysts and glass in ash from the 2004 eruption of Mount St. Helens for major- and trace-elements to identify juvenile material and explore methods of ash generation over the course of the eruption.

The Role of Subduction Fluids in Generating Compositionally Diverse Basalts in the Cascadia Subduction Zone

by
Michael C. Rowe

A DISSERTATION

submitted to

Oregon State University

in partial fulfillment of
the requirements for the
degree of

Doctor of Philosophy

Presented April 27, 2006
Commencement June 2006

Doctor of Philosophy dissertation of Michael C. Rowe presented April 27, 2006.

APPROVED:

Co-Major Professor, representing Geology

Co-Major Professor, representing Geology

Chair of the Department of Geosciences

Dean of the Graduate School

I understand that my dissertation will become part of the permanent collection of Oregon State University libraries. My signature below authorizes release of my dissertation to any reader upon request.

Michael C. Rowe, Author

ACKNOWLDEGEMENTS

I would like to thank Roger Nielsen and Adam Kent for guiding me towards the completion of my dissertation and for keeping me funded for these past 5 years. Funding for the majority of this dissertation was provided by an NSF grant to Dr. Nielsen and Dr. Kent and through two Geological Society of America student research grants and a Kleinman research grant through the US Geological Survey. I would also like to thank Anita Grunder and Dave Graham for continued discussions of Cascade petrology and geochemistry and for serving on my committee. This research would not have been possible without the databases of published and unpublished whole rock data for the Oregon Cascades and Newberry vicinity provided by Rick Conrey and Dave Sherrod. In addition, Carl Thornber's help with the Mount St. Helens ash project was instrumental and I greatly appreciate his willingness to involve me with the current eruptive events. Lastly I would like to acknowledge my parents, Jerry and Sandy Rowe, and wife and son, Kristin and Christopher, for their ongoing support in completing this dissertation.

CONTRIBUTION OF AUTHORS

Dr. Adam Kent and Dr. Roger Nielsen provided oversight for all three Oregon Cascade manuscripts. Dr. Roger Nielsen provided training and assistance with electron microprobe techniques and experimental techniques for one-atmosphere melt inclusion rehomogenization. Dr. Adam Kent assisted with collection of trace element data by laser-ablation ICP-MS analysis of melt inclusions. Dr. Carl Thornber (USGS-Cascade Volcano Observatory) provided access to samples and discussion of results for the Mt. St. Helens manuscript.

TABLE OF CONTENTS

TABLE OF CONTENTS (Continued)

TABLE OF CONTENTS (Continued)

TABLE OF CONTENTS (Continued)

TABLE OF CONTENTS (Continued)

LIST OF FIGURES

LIST OF FIGURES (Continued)

LIST OF FIGURES (Continued)

LIST OF FIGURES (Continued)

LIST OF TABLES

LIST OF APPENDIX TABLES

LIST OF APPENDIX TABLES (Continued)

LIST OF APPENDIX FIGURES

THE ROLE OF SUBDUCTION FLUIDS IN GENERATING COMPOSITIONALLY DIVERSE BASALTS IN THE CASCADIA SUBDUCTION ZONE

CHAPTER 1

GENERAL INTRODUCTION

For decades subduction zones have been the target of detailed petrologic, geochemical, and geophysical studies. A major goal of many studies has been to examine geochemical recycling resulting from subduction of oceanic lithosphere, including overlying sediments and crust, into the upper and lower mantle. Subduction zones are also important regions of crustal growth and recycling. By studying the inputs and outputs of subduction zone processes (arc volcanism) researchers ultimately attempt to quantify the chemical composition of the continental crust and the residual recycled material, critical for understanding its potential role as a driving force of mantle heterogeneity and as a means of recycling volatile phases to the mantle (i.e. Armstrong, 1968; Karig and Kay, 1981; Hofmann and White, 1982; Tatsumi, 2005; Wallace, 2005). Despite this intense focus, many questions still remain unanswered as a result of the complex array of tectonic and petrologic processes that affect arc lava compositions. These include fundamental questions regarding the thermal structure and fO_2 of the subarc mantle, which have the potential to exert significant control on the generation of subduction zone magmas (i.e. Stern, 2002).

Traditional models of subduction zone processes revolve around the subduction of oceanic sediments, crust and lithospheric mantle which undergo phase transformations and dehydration as a result of increasing pressure and temperature (Schmidt and Poli,

1998; Harry and Green, 1999). Hydrous fluids or melts (generally referred to as the subduction component) derived from these phase transformations migrate into the convecting subarc mantle, lowering the mantle solidus and generating basaltic magmas (i.e. Tatsumi et al., 1986). These basaltic magmas commonly inherit an enrichment in fluid-mobile and/or incompatible elements (i.e. Cl, Ba, K, Na, La, Pb, Sr, U, Rb, Th) likely transported as part of the subduction component (Stolper and Newman, 1994).

Understanding the petrogenesis of subduction zone basalts is complicated by the common occurrence of multiple, distinct basaltic compositions within arc settings (e.g. Conrey et al., 1997; Bacon et al., 1997; Churikova et al., 2001). These often have major- and trace-element and isotopic characteristics which require a mineralogically and compositionally heterogeneous subarc mantle and/or several different methods of melt generation, thus further complicating interpretations (Walker et al., 2003; Conrey et al., 1997; Stolper and Newman, 1994).

The thicker (typically greater than 40km) crust of continental arcs provides additional complications to understanding subduction zone processes. Assimilation and fractional crystallization have the potential to greatly modify a primary melt composition. In addition, trace element signatures similar to those considered characteristic of a subduction component, can also result from assimilation of arc crust as this material is likely generated in a similar fashion to the basaltic magmas under examination (Davidson, 1996).

The overall goal of this study is to utilize major-, trace-, and volatile element variability in conjunction with basaltic oxygen fugacity (fO_2) to evaluate the effects of

addition of a subduction component to the subarc mantle in the Cascade subduction zone in the generation of basaltic magmas. In order to approach this problem we have selected the most primitive basaltic lavas (>6-8 wt% MgO; and olivine Fo# >75) from a transect across the central Oregon Cascades (between 43-45°N), providing the opportunity to study both spatial and compositional variability with regard to basalt petrogenesis. To reduce the potential impact of crustal processes and to allow us to study volatile element abundances we have focused on olivine-hosted melt inclusions from the most primitive available.

Melt inclusions, small packets of melt trapped within phenocrysts during crystallization, have become an important tool for petrologic and volcanologic studies (e.g. Cervantes and Wallace, 2003; Danyushevsky et al., 2002; Kent et al., 2002; Nielsen et al, 1995; Saal et al. 1998; Sisson and Layne, 1993; Sobolev and Shimizu, 1993), providing constraints on primitive melt composition, volatile concentration, and temperature at the time of entrapment within the host phenocryst phases. There are several advantages to utilizing melt inclusions in the Oregon Cascades. Since the crust beneath the Cascades is relatively thick (~45 km), there is an increased likelihood of significant crustal assimilation during melt transport (Stanley et al., 1990). Focusing this study on the most primitive inclusions, which have essentially been chemically isolated from the rest of the magma since entrapment, reduces the impact of assimilation on the composition of the primitive melt. As inclusions are likely trapped at different times in the evolution of the basalt, they provide the opportunity to address the amount of modification the basaltic magmas have undergone by examining the variability of the

inclusion compositions with respect to the host lava. In addition, because subaerial eruptions undergo extensive degassing prior to eruption, volatile contents from erupted basalts are extremely low and unrepresentative of the original magmatic volatile content. Due to their isolation within crystalline phases at relatively high pressures, inclusions have the potential to retain volatiles (S, Cl, H_2O, CO_2) despite degassing of the magma, thus providing important variables for modeling magma petrogenesis that would otherwise be unobtainable.

The use of melt inclusions to constrain primitive compositions is not without complication however, as inclusions may also undergo a range of post-entrapment modification potentially resulting in significant changes to an inclusions composition (Danyushevsky et al., 2002). In slowly cooling lavas, melt inclusions may experience crystallization similar to that of the host basalt, resulting in the crystallization of 1) the host mineral on the inclusion-phenocryst boundary and 2) daughter crystals within the inclusion. In order to recreate the melt compositions at the time of entrapment we must rehomogenize (re-melt crystals and rapidly cool to form a glass) the inclusions, ideally producing a glass composition similar to that of the initially trapped liquid. This also provides a homogenous glass that we may analyze by microanalytical techniques (electron microprobe and laser ablation (LA) ICP-MS) to determine major-, trace-, and volatile element concentrations.

A further emphasis of this study is determining the fO_2 of Cascade basalts and providing constraints on the oxidation state of the subarc mantle. Direct measurement of mantle fO_2 is limited to mantle xenoliths which may be rare in some volcanic settings. In

some cases, this has led to generalizations about the fO_2 of the subarc mantle based on relatively few constraints (Brandon and Draper, 1996). In this study we determine the oxidation state of primitive basalts directly from the speciation of sulfur retained within the melt inclusions. Utilizing the calculated oxygen fugacity of the primitive basalts we may then determine the potential influence of a subduction component to the mantle wedge beneath the volcanic arc.

The first manuscript of this thesis (Chapter 2) is dedicated to documenting a previously unidentified post-entrapment modification resulting in excess FeO* observed in melt inclusions from absarokitic/shoshonitic basalts in the Cascade forearc. In addition to the crystallization previously described, numerous post-entrapment modifications have the ability to significantly alter the composition of a melt inclusion. Two such processes which are commonly observed are Fe-loss and hydrogen diffusion (Danyushevksy et al., 2002; Hauri, 2002; Qin et al., 1996). Fe-loss results from the re-equilibration of the host olivine with the melt at high temperatures, causing an increase in MgO wt% and a decrease in FeO wt% in the melt (Danyushevksy et al., 2000). Hydrogen diffusion has been documented in melt inclusions which have experienced extended periods of rehomogenization or heating. In these cases, water in inclusions will dissociate and hydrogen will diffuse rapidly out of the olivine host resulting in excess oxygen in the melt inclusion, changing the fO_2 of the inclusion. In the example of our forearc inclusions, melt compositions have anomalously high FeO contents (up to 21 wt% FeO), significantly greater than that observed in the bulk lava (6.66 wt% FeO). This

chapter therefore documents rehomogenization experiments designed to determine the source of the anomalous FeO* concentrations.

In the course of improving methods of measuring sulfur speciation in melt inclusions it became evident that the oxidation state of the inclusion and thus the sulfur speciation could change, both as a result of natural processes and during rehomogenization and measurement (Sato and Wright, 1966; Mathez, 1984; Danyushevsky et al., 2002). The third chapter of this thesis details an experimental study to evaluate the potential effects of degassing, fractional crystallization, melting, post-entrapment modification (i.e. Fe-loss and hydrogen diffusion), and rehomogenization on sulfur speciation. This study was necessary to document these variations which had previously gone unnoticed or ignored, in order to justify the application of this technique to melt inclusions in the Oregon Cascades.

The fourth chapter of this thesis details the application of rehomogenization techniques and sulfur speciation measurements to examine the across-arc variability in melt inclusion composition and oxidation state in primitive basalts from the central Oregon Cascades (Fig. 1). Using representative samples of distinct basalt compositions from the backarc, arc, and forearc, I hope to be able to constrain the source oxygen fugacity for each of the respective basalt types and as we have samples spanning over ~100 km across the arc, include a spatial interpretation with respect to the subarc mantle oxidation state. Lastly, by combining the calculated oxygen fugacity with trace- and volatile-element concentrations I can investigate the effect of addition of a subduction component to the mantle wedge and how that influences basalt geochemistry.

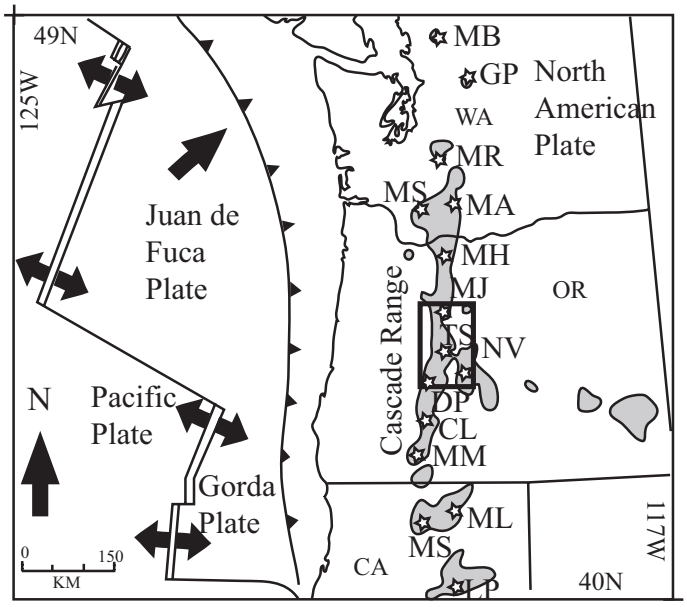

Figure 1: Location of study region within the central Oregon Cascades from ~ 43-45 degrees N (bold outline). Major volcanic centers (stars) are (from N to S): Mt. Baker (MB), Garibaldi Pk. (GP), Mt. Rainier (MR), Mt. St. Helens (MS), Mt. Adams (MA), Mt. Hood (MH), Mt. Jefferson (MJ), Three Sisters (TS), Newberry Volcano (NV), Diamond Pk. (DP), Crater Lk. (CL), Mt. McLoughlin (MM), Mt. Shasta (MS), Medicine Lk. (ML), Lassen Pk. (LP). Shaded fields on map represent volcanic vents younger than 1 Ma (modified from Guffanti and Weaver, 1988). Juan de Fuca plate motion vector relative to North America is from Riddihough (1984).

Over the course of this study the opportunity also arose to apply similar electron microprobe and LA-ICP-MS techniques to the 2004 eruption of Mount St. Helens, WA. The final chapter included in this thesis documents geochemical analysis of ash samples collected from Mt. St. Helens during 2004 and 2005, identifying and quantifying juvenile contributions to ash produced by phreatomagmatic explosions and dome collapse events.

Detailed analytical methods and complete tables of data utilized in this study are provided in the appendices.

CHAPTER 2

ANOMALOUSLY HIGH FE CONTENTS IN REHOMOGENIZED OLIVINE HOSTED MELT INCLUSIONS FROM OXIDIZED MAGMAS

Michael C. Rowe
Roger L. Nielsen
Adam J. R. Kent

American Mineralogist
Mineralogical Society of America
3635 Concorde Pkwy Suite 500
Chantilly, VA 20151-1125
Volume 91, pages 82-91, 2006

ABSTRACT

Iron concentrations in rehomogenized (remelted) melt inclusions hosted in forsterite-rich olivine (Fo_{88-92}) from an alkalic lava have significantly higher Fe contents (FeO* up to 21 wt%) than found in naturally quenched inclusions, matrix glasses, and bulk lava compositions (6.21-6.66 wt% FeO*). The main objectives of this study are to (1) determine the source of the anomalous Fe concentrations and (2) evaluate the significance of this signature with respect to rehomogenization of melt inclusions. Heating experiments conducted from 1125ºC to 1225ºC on crystallized inclusions show that Fe and Mg contents in rehomogenized inclusions increase with homogenization temperature, consistent with dissolution of olivine + magnetite in a 1:1 atomic ratio. The dissolution of magnetite contributes significant excess Fe to the homogenized inclusions, and thus the high FeO* contents of the glasses do not reflect the original composition of the trapped melt. The addition of excess Fe also dilutes the concentrations of other major elements, especially evident in SiO_2, Al_2O_3, and CaO wt%.

While the cause of magnetite formation in the inclusions is unresolved, two models (hydrogen diffusion and co-entrapment of magnetite) for the formation of significant volumes of magnetite are considered. One of the most significant conclusions for this study is that magnetite formation occurred prior to rehomogenization and that the magnetite did not result from post-entrapment fractional crystallization of the inclusion. For these inclusions, a correction must be made for the dissolution of magnetite (± pyroxene) and olivine to the silicate melt to accurately reconstruct the original Fe content of the melt.

INTRODUCTION

Over the past 15 years, melt inclusions have become an important tool for petrologic and volcanologic studies (e.g. Cervantes and Wallace, 2003; Danyushevsky et al., 2002; Kamenetsky et al., 1997; Kent et al., 2002; Nielsen et al, 1995; Saal et al. 1998; Sisson and Bronto, 1998; Sisson and Layne, 1993; Sobolev and Shimizu, 1993) providing direct (and indirect) constraints on primitive melt composition, volatile concentration, and temperature at the time of entrapment within phenocryst phases. One important issue that must be dealt with for study of many melt inclusions is that of post entrapment crystallization and the need to accommodate the effects of the crystallization of a range of daughter mineral phases. In addition, even where inclusions may appear glassy, substantial crystallization of the host mineral onto the walls of the inclusion commonly also occurs (Danyushevsky et al., 2002). In order to reconstruct the composition of the trapped melt by re-equilibrating the trapped melt with the host mineral, and to provide a homogenous glass for microbeam-based analytical techniques, crystallized inclusions are often rehomogenized. This involves reheating the phenocrysts to the melt liquidus (trapping) temperature to re-dissolve daughter crystals and crystallized host mineral into the melt, followed by rapid cooling to quench to a glass. Rehomogenization is typically done using a high temperature microscope stage (Danyushevsky et al., 2002), or via heating of mineral grains containing inclusions at controlled redox conditions in a 1 atm furnace (e.g. Nielsen et al., 1998; Danyushevsky et al., 2002). Both techniques have their advantages and disadvantages: rehomogenization by microscope heating stage requires

specialized equipment and is less time-efficient – as it is limited to heating individual grains during a single experiment, whereas furnace heating uses more widely available equipment (generally gas-mixing furnaces) and allows treatment of multiple grains (up to several 100 depending on grain size) at a time. However, microscope heating stages allow direct observation of each inclusion as it homogenizes, providing a means to measure the trapping temperature and information about the liquid line of descent (Danyushevsky et al., 2002). Rehomogenizing via a furnace requires that the trapping temperature be independently estimated, and all inclusions in a single experiment are homogenized at the same temperature. Moreover, it is also generally assumed that small differences between the homogenization temperature and that of inclusion trapping can be corrected for numerically by addition or subtraction of the host mineral until equilibrium is obtained. For olivine-hosted inclusions this correction is generally done by incrementally adding or subtracting olivine until the inclusion and host mineral are in Fe-Mg exchange equilibrium (e.g., Sobolev and Chaussidon, 1996), however this also assumes that compositional changes in the inclusion over a range of homogenization temperatures are only controlled by equilibrium with the host mineral.

In addition, and regardless of the heating method used, previous studies have also identified several further complications that may arise both through re-equilibration prior to eruption and during rehomogenization of olivine-hosted melt inclusions (Nielsen et al., 1998; Gaetani and Watson, 2000; Danyushevsky et al., 2000, 2002). Inclusions that are "breached" or open during reheating may lose or gain chemical components (Nielsen et al., 1998). Fe-loss may occur via relatively rapid diffusion of Fe through the host olivine

following crystallization of Fe-rich olivine on the interior of inclusions (Danyushevsky et al., 2000, 2002). In addition, volatile concentrations can be significantly modified by diffusion of hydrogen through the host olivine (Qin et al., 1992; Hauri, 2002; Danyushevsky et al., 2002). Despite these complications, melt inclusions still provide one of the few direct methods for determining primitive compositions prior to extensive crystallization, mixing and degassing, especially in subaerially erupted lavas where volcanic gasses are lost during eruption.

In this study we report an example of Fe-gain in rehomogenized olivine-hosted melt inclusions, an additional complication that can arise – particularly in oxidized and water-rich mafic magmas. Although increased Fe contents in homogenized melt inclusions have previously been attributed to melting of mineral inclusions trapped together with melt (e.g. Kent and Elliott, 2002), to our knowledge Fe-gain of this type has not yet been documented in detail in the melt inclusion literature. Therefore, the goal of this study is to (1) identify the source of the excess Fe and (2) determine the extent to which this affects our ability to reconstruct original melt compositions during rehomogenization.

SAMPLE DESCRIPTION

Samples collected for this study are from a basaltic lava flow (Lat. 44º36.047'N, Long. 122º 20.146'W) and scoria cone (Lat. 44º36.012'N, Long. 122º18.896'W) in the Quartzville mining district located on the western margin of the Oregon Cascades. Detailed field mapping shows that scoria and lava samples are contemporaneous and Ar-Ar age dating indicates an eruption age of 82.3 ± 3.1 ka (Rowe, M.C., unpublished data).

This conclusion is also supported by chemical and petrologic similarities between lava and scoria (Table 1). The phenocryst phases present in the lava and scoria are olivine, clinopyroxene, magnetite, and trace microapatites (< 35 μm). Cr-spinel is an important constituent present dominantly as a mineral inclusion within the olivine phenocrysts. Rounded quartz xenocrysts are also present in the lava and gabbroic xenoliths have been previously reported from the lava flow (Conrey et al., 1997). Melt inclusions in unheated olivine phenocrysts from the lava flow are generally oval shaped, containing residual glass ± clinopyroxene ± coarse grained magnetite (up to 25μm in diameter). Textures of unheated inclusions vary from dominantly crystallized with coarse cpx and magnetite with little residual glass to mostly glassy, however still containing coarse magnetite. Melt inclusions trapped within olivine phenocrysts from the scoria sample are typically round to oval-shaped, and consist entirely of glass (no daughter crystals evident).

METHODS

Olivine phenocrysts were hand-picked from lightly crushed samples of lavas and scoria. To rehomogenize inclusions, phenocrysts were heated in a 1 atm vertical quench Deltec furnace. Olivine grains (~50/temperature increment) were wrapped in platinum foil and suspended in the vertical furnace by platinum wire. Oxygen fugacity was maintained at the QFM oxygen buffer with a mixture of H_2 and CO_2 gas. Olivine grains were heated rapidly (~2-3 minutes) to the maximum run temperature, where they were held for 15 minutes followed by rapid quenching in water. The relatively short rehomogenization times are based on the experimental work of Danyushevsky et al.

(2000, 2002) and Hauri (2002) which document Fe-loss and hydrogen diffusion occurring during longer homogenization times. Olivines were rehomogenized at run temperatures of 1125ºC, 1150ºC, 1175ºC, 1200ºC, and 1225ºC. Heated olivines, as well as a selection of unheated olivine from lava and scoria, were mounted in 25 mm epoxy disks and polished to expose the grain interiors.

The major element (and for glasses, S and Cl) contents of melt inclusions, olivine host phenocrysts, Cr-spinel inclusions, and magnetite crystals were measured via electron microprobe using a Cameca SX50 and SX100 at Oregon State University. Olivine, Cr-spinel, and magnetite grains were analyzed using a focused (1μm) beam, with a 15 KeV accelerating voltage and 50 nA beam current. Melt inclusion analyses were made with a beam diameter of 4-7μm (dependent on inclusion size) with a 15 KeV accelerating voltage and 30 nA beam current. Mineral standards [San Carlos olivine (USNM 11312/444), chromite (USNM 117075), and Minas Gervais magnetite (USNM 114887), and glass standard Makaopuhi Lava Lake basaltic glass (USNM 113498/1 VG-A99)] were analyzed 3-5 times prior to each analytical run. Determination of the oxidation state of the rehomogenized melt inclusions was made by S Kα peak shift determinations following the procedure of Carroll and Rutherford (1988) and Wallace and Carmichael (1994). Peak shift determinations were made on a Cameca SX50 microprobe at the University of Oregon.

Major- and trace-element concentrations in the lava were determined by XRF and ICP-MS, respectively, at Washington State University (Johnson et al., 1999). Five melt inclusions, rehomogenized at 1200ºC, were analyzed by laser ablation (LA) ICP-MS at

Oregon State University. Additionally, 10 analyses of the scoria glass and 5 analyses of BHVO-2G standard glass, were made by LA-ICP-MS (Table 2).

Trace element concentrations in melt inclusions and glasses were determined by LA-ICP-MS in the W.M. Keck Collaboratory for Plasma Spectrometry, Oregon State University. Analyses were performed using a NewWave DUV 193 nm ArF Excimer laser and VG PQ ExCell Quadrupole ICP-MS under conditions similar to that reported in Kent et al. (in press). Ablation was carried out using He as the carrier gas, and this was mixed with Ar immediately prior to the plasma torch. Background count rates were measured for 30 s before ablation commenced for each analysis. Plasma torch conditions were optimized so that ThO/Th ratios were < 2%. Analyses were performed using the spot mode – using a stationary laser to progressive ablate a progressively deepening crater in the sample materials. Each individual analysis represents 40 s data acquisition during ablation using 50 and 80 μm spot for inclusions and glass respectively, and with pulse frequency of 4 Hz, resulting in an ablation crater ~15 μm deep. Trace element abundances were calculated relative to the USGS glass standard BCR-2G, which was analyzed under identical conditions throughout the analysis session (see Kent et al. in press for the values used for calibration). ^{43}Ca was used as the internal normalizing isotope in conjunction with CaO contents measured by electron microprobe. USGS glass BHVO-2G was also analyzed to monitor accuracy and precision. Results are shown in Table 2, and show excellent agreement with published compositions.

RESULTS

A total of 138 melt inclusions were analyzed from rehomogenization experiments. Of these, 84 had measured sulfur concentrations at or above the sulfide saturation curve defined by Wallace and Carmichael (1992) and are therefore interpreted not to have degassed at low pressure during eruption or during laboratory rehomogenization (Nielsen et al., 1998). Low Cl concentrations observed in the inclusions that plot below the S saturation curve support the contention that these inclusions have been degassed. Although Fe/Mg ratios are consistent between the degassed (0-500 ppm S) and high S (>700 ppm) melt inclusions, only the high S inclusions (unbreached) are discussed further in order to avoid inclusions which may have had post-entrapment interaction with the magma during ascent or contamination during rehomogenization.

Total FeO (FeO*) concentrations from naturally quenched melt inclusions from scoria contain broadly similar FeO* contents of 6.7 ± 0.8 wt% FeO* (1 standard deviation), consistent with those of the bulk lava and scoria glass (6.53 and 6.22 wt% FeO*, respectively; Table 1). In contrast, rehomogenized melt inclusions from the lava have variable, and typically significantly higher, Fe contents, up to 21 wt% FeO*. In general, average FeO* and MgO contents increase with temperature (Figs. 1, 2), and the FeO*/MgO ratios also increases from those measured in scoria and naturally glassy inclusions (~1.4) to inclusions rehomogenized at 1175-1225ºC (~ 2.0). In contrast, SiO_2 and Al_2O_3 decrease significantly with temperature while CaO, Na_2O, K_2O, and P_2O_5 remain relatively constant, consistent with dilution (Fig. 2; Table 1).

Sulfur concentrations in naturally quenched inclusions from the scoria sample vary from 0.09 to 0.32 wt % S. A positive correlation to water, estimated by difference from

Table 1. Host lava, scoria and melt inclusion major element analyses.

	Hosts		Melt Inclusions		
Sample	Lava†	Scoria‡	Nat. quenched	mesostasis	1125(°C)
N=	1	15	16	4	5
SiO_2	50.06	51.06 (51.51-50.43)	50.61 (51.96-48.77)	63.84 (64.87-62.78)	51.25 (53.04-48.90)
Al_2O_3	13.64	16.74 (17.08-16.33)	15.63 (17.15-15.02)	14.57 (17.37-12.97)	12.81 (16.38-9.92)
TiO_2	1.581	1.74 (1.79-1.68)	1.82 (1.97-1.47)	0.96 (1.46-0.67)	1.06 (1.57-0.62)
FeO*	6.53	6.21 (6.38-5.83)	6.66 (7.55-4.30)	2.69 (3.43-2.05)	10.03 (12.83-7.34)
MnO	0.105	0.11 (0.16-0.05)	0.10 (0.15-0.04)	0.02 (0.05-0.00)	0.08 (0.10-0.05)
CaO	10.14	8.72 (10.04-8.00)	10.54 (13.25-3.82)	4.27 (7.72-2.08)	10.47 (12.92-8.98)
MgO	9.86	4.59 (4.93-4.29)	4.67 (5.80-2.49)	3.46 (5.37-1.24)	6.65 (9.47-5.06)
K_2O	3.11	3.40 (3.77-2.70)	1.89 (2.66-1.31)	1.67 (2.52-1.20)	2.20 (3.59-0.47)
Na_2O	2.88	3.91 (4.01-3.77)	2.25 (3.89-1.43)	3.64 (4.82-2.72)	2.92 (3.64-2.26)
P_2O_5	1.173	1.31 (1.37-1.24)	1.26 (1.38-0.42)	0.81 (1.26-0.56)	1.14 (1.53-0.03)
S	-	0.27 (0.38-0.23)	0.42 (0.60-0.09)	0.16 (0.24-0.11)	0.18 (0.33-0.07)
Cl	-	0.16 (0.18-0.14)	0.15 (0.19-0.08)	0.12 (0.15-0.07)	0.07 (0.10-0.01)
Total	99.07	98.25 (98.95-97.40)	96.00 (97.05-94.55)	96.22 (97.34-95.68)	98.85 (101.16-98.06)
FeO*/MgO	0.66	1.35 (1.41-1.27)	1.43 (1.82-1.19)	0.78 (2.77-0.38)	1.51 (2.45-1.06)
$Kd_{ol\text{-}melt}$	0.35	0.22 (0.23-0.21)	0.20 (0.29-0.15)	0.36 (0.09-0.62)	0.18 (0.24-0.12)
Host Fo#	90.6	89.2 (90.2-86.1)	89.2 (90.2-86.1)	90.6 (91.0-89.4)	90.1 (90.5-88.9)

Note: Only melt inclusions which retained sulfur concentrations at or above the S-saturation curve (N) are used for defining average
compositions at each heating increment. Naturally quenched inclusions are from the scoria sample. See text for discussion of determination of $Kd_{olivine\text{-}melt}$. Parentheses indicate the range in compositions observed at each temperature interval (high-low).

* FeO as total iron.

† Bulk rock XRF analyses performed at Washington State University (Johnson et al., 1999).

‡ Scoria glass composition determined by electron microprobe analysis.

Table 1: Continued.

	Melt Inclusions			
Sample	1150(ºC)	1175 (ºC)	1200 (ºC)	1225 (ºC)
N=	7	7	38	8
SiO_2	51.80 (58.13-46.80)	49.61 (61.42-45.10)	46.46 (57.87-41.89)	45.94 (52.72-42.75)
Al_2O_3	12.85 (14.28-11.60)	12.33 (13.89-10.39)	11.66 (13.67-9.47)	11.12 (12.08-9.79)
TiO_2	1.08 (1.60-0.72)	1.06 (1.57-0.62)	1.13 (1.59-0.42)	1.06 (1.40-0.72)
FeO*	9.06 (11.80-4.93)	12.91 (17.05-5.61)	14.44 (19.87-7.53)	16.16 (21.67-9.61)
MnO	0.06 (0.13-0.00)	0.08 (0.19-0.04)	0.08 (0.13-0.02)	0.09 (0.12-0.02)
CaO	9.45 (11.98-7.34)	8.84 (10.45-7.35)	9.13 (11.62-2.69)	8.51 (9.97-7.52)
MgO	6.57 (7.72-5.61)	6.67 (7.55-5.93)	7.25 (9.56-4.74)	8.19 (9.09-7.08)
K_2O	3.12 (3.78-2.71)	2.95 (3.10-2.42)	3.03 (5.03-2.54)	2.80 (3.22-2.56)
Na_2O	2.71 (3.16-2.41)	2.67 (2.82-2.30)	2.77 (4.33-1.94)	2.43 (2.73-2.12)
P_2O_5	1.29 (1.69-1.02)	1.16 (1.60-0.94)	1.18 (1.72-0.86)	1.05 (1.28-0.87)
S	0.29 (0.57-0.11)	0.31 (0.58-0.07)	0.56 (0.92-0.14)	0.53 (0.84-0.13)
Cl	0.10 (0.11-0.08)	0.08 (0.11-0.04)	0.10 (0.14-0.03)	0.10 (0.13-0.06)
Total	98.39 (99.34-97.79)	98.67 (100.23-97.15)	97.80 (101.07-95.66)	97.98 (99.17-97.60)
FeO*/MgO	1.38 (1.99-0.64)	1.94 (2.79-0.95)	1.99 (3.23-1.10)	1.97 (3.06-1.06)
$Kd_{ol\text{-}melt}$	0.19 (0.36-0.13)	0.14 (0.26-0.09)	0.13 (0.23-0.07)	0.13 (0.21-0.09)
Host Fo#	90.9 (92.2-90.1)	90.8 (91.7-89.5)	90.5 (91.6-89.6)	90.6 (91.4-89.2)

electron microprobe totals (100-analytical total), suggests that the S variability in naturally quenched inclusions from the scoria cone is due to degassing, likely during eruption. Mesostasis from lava samples and inclusions rehomogenized between 1125°C and 1150°C tend to have sulfur concentrations that are just above the sulfide saturation curve with concentrations ranging from 0.06 wt% to 0.3 wt% (Wallace and Carmichael, 1992). The lower sulfur concentrations in the mesostasis glass likely reflect the lower sulfur solubility with increasing SiO_2 and decreasing FeO. Melt inclusions rehomogenized at higher temperatures (1200-1225°C) define a positive correlation between Fe and S with sulfur concentrations ranging from 0.35 to 0.9 wt% S (Fig. 3c). Despite this trend, there is a wide range of sulfur concentrations with respect to FeO* in the rehomogenized melt inclusions at similar temperatures (Fig. 3c). S Kα peak shift analysis of melt inclusions rehomogenized at 1200ºC indicates an oxidation state relative to the Ni-NiO buffer of ΔNNO + 0.5 (Wallace and Carmichael, 1994).

Trace-element concentrations of the rehomogenized inclusions do not show a significant variation from either the scoria or lava analyses. In general, the inclusions are enriched in LILE (Ba, Sr, U, Th) and LREE (La, Ce) with a strong depletion, relative to the more mobile elements, in Ti, Y, Yb, Nb and Ta (see discussion). Trace element data is summarized in table 2.

Olivine compositions from the scoria range from $Fo_{88.2}$ to Fo_{90} with Ni concentrations varying from 0.25 to 0.62 wt% NiO. Oxides found as inclusions in the olivine phenocrysts are Cr-Mg-Al rich spinels. Spinel compositions are relatively constant with a Mg# of ~ 62 and Cr# of ~76 (Table 3). The compositions of olivine phenocrysts from

Figure 2: Major element analyses versus temperature of rehomogenization. (a) FeO* and (b) MgO both generally increase with increasing temperature while (c) SiO_2 and (d) CaO decrease with increasing temperature. Large symbols are average compositions with 1 standard deviation error bars. Dashed lines represent dilution of bulk lava (corrected for 6 wt% accumulated olivine) by the addition of excess FeO* and MgO.

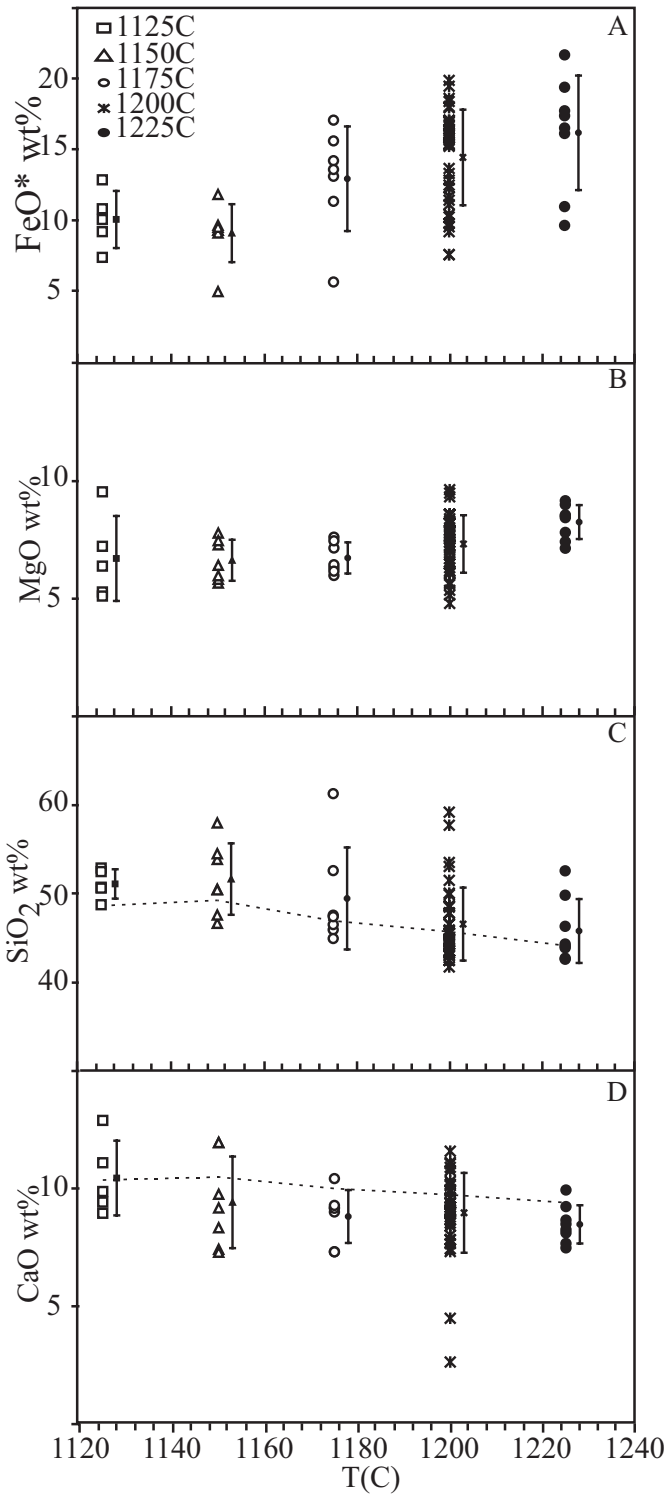
1125C
1150C
1175C
1200C
1225C
A
FeO* wt%
20
15
10
5
B
MgO wt%
10
5
C
SiO2 wt%
60
50
40
D
CaO wt%
10
5
1120
1140
1160
1180
1200
1220
1240
T(C)

Figure 2.

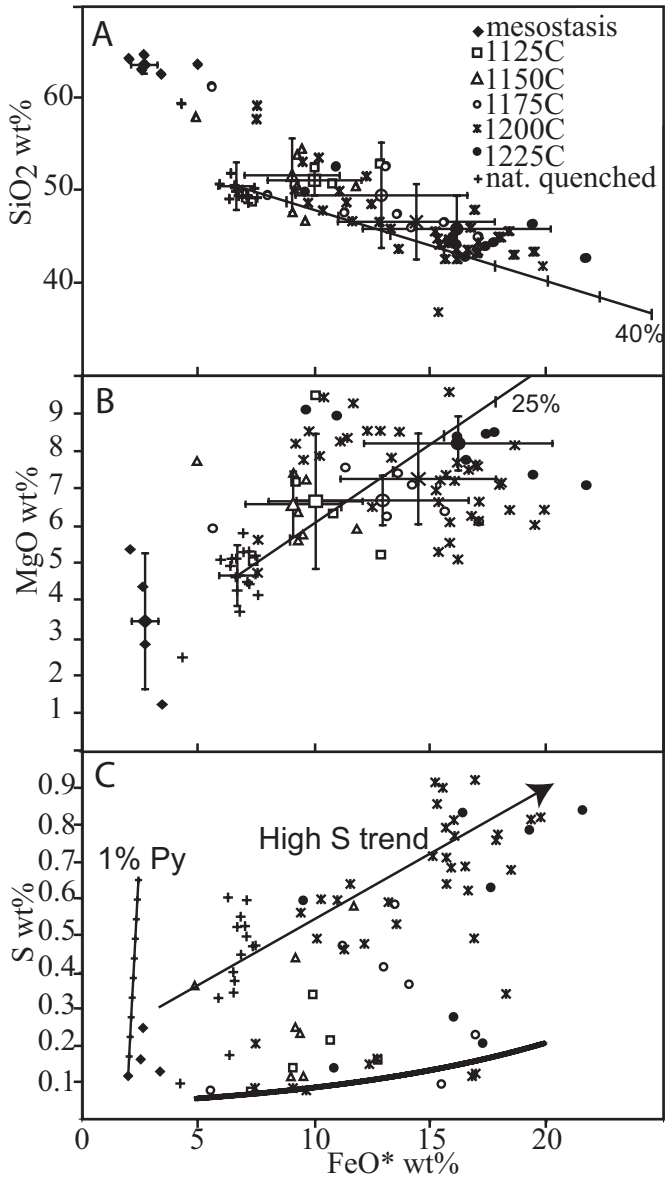

Figure 3: (a) SiO_2 versus FeO illustrating the decreasing SiO_2 concentration with increasing FeO* and temperature. (b) MgO and FeO both increase with increasing temperature. Large symbols are average compositions (Table 1) with error bars representing 1 standard deviation. Solid lines represent the addition of a 1:1.6 (wt% ol-mt) mixture to the naturally quenched inclusion average composition in 5% increments. (c) S wt% versus FeO* wt%. Bold line is the sulfide saturation curve from Wallace and Carmichael (1994) and the thin line illustrates the addition in the S/FeO* ratio of 1 wt% pyrite into the silicate melt. Arrow delineates high S trend observed dominantly in the 1200°C-1225°C inclusions (see text).

the lava flow range between $Fo_{89.4}$ and $Fo_{92.2}$ and have Ni concentrations that vary from 0.31 to 0.82 wt% NiO with increasing forsterite content. Repeat analyses (n=10) of the San Carlos olivine standard (0.38 ± 0.03 NiO wt % measured, 0.37 wt% accepted) and a high NiO olivine (0.82 ± 0.08 NiO wt%) confirms that the high NiO concentrations are not an analytical artifact and to the authors knowledge are the highest Ni concentrations reported for olivine compositions. Two different oxide phases occur trapped within the olivine hosted melt inclusions. Cr-Mg-Al rich spinels are found as inclusions coexisting with silicate melt and as mineral inclusions in host olivine phenocrysts (Fig. 4, 5). These have Mg#'s from 52.2 to 65.6 (avg. 58.3 ± 3.1) and Cr#'s from 68.5 to 91.5 (avg. 76.8 ± 4.7), similar to those found in as mineral inclusions in the olivines from the scoria. Spinel mineral inclusions from the lava flow are generally slightly lower in Al_2O_3 and TiO_2, suggesting that these spinels may have formed from a slightly more primitive melt than those found in the scoria sample, consistent with the observation that the scoria is slightly more evolved than the basaltic lava (Kamenetsky et al., 2001). In addition, magnetite grains, with up to 80 wt % FeO* and minor Cr concentrations are found trapped together with silicate melt in both unheated and heated olivines from the lava flow, but are not observed as mineral inclusions within the olivine phenocrysts. A solid-solution is observed between magnetite and chromite in the olivines from the lava, consistent with experimental work by Katsura and Muan (1964) and Lindsley (1976), however magnetites are only found in the inclusions from lava-hosted olivines, Cr-rich spinels are the only oxide phase that has been identified in the scoria-hosted olivines and inclusions.

Table 2. Melt Inclusion and host LA-ICP-MS trace-element concentrations.

Sample	Melt Inclusions					Hosts		Standard	
ID (N)	03-38-14.1	03-42-5.1	03-43-15.1	03-63-5.1	03-61-3.1	Scoria (10)	Lava†	BHVO-2G (5)	Dev. (%)
Concentration (ppm)									
Sc	15.7	16.7	18.2	20.4	14.9	9.97	23.5	29.3	0.5
Ti	8336	6869	7248	7116	6541	7928	-	16502	48
V	159	337	158	-	-	167	140‡	328	2
Zn	-	-	-	-	-	85.5	98‡	107	1
Rb	38.4	91.2	36.8	27.5	26.3	33.7	26.9	10.0	0.2
Sr	4132	2406	4147	2863	2890	3275	3124	414	9
Y	22.3	24.7	20.4	14.8	14.6	15.2	20.6	24.1	0.6
Zr	436	366	397	276	284	294	336	159	4
Nb	9.72	14.2	9.13	6.90	7.29	8.09	7.23	20.6	0.4
Ba	2684	1955	2638	2140	1928	2162	2242	143	3
La	91.8	117	88.7	64.8	67.1	77.0	83.9	15.9	0.3
Ce	225	298	236	186	183	193	185	41.7	0.8
Pr	29.8	36.7	31.2	23.4	23.6	25.4	24.4	5.68	0.13
Nd	115	141	118	83.6	90.1	97.7	100	24.6	0.9
Sm	17.4	23.2	20.9	12.8	14.2	14.8	17.5	6.05	0.17
Eu	4.74	5.54	5.95	3.35	3.82	3.90	4.59	2.10	0.05
Gd	9.68	10.4	8.80	8.06	7.70	8.31	10.4	5.91	0.10
Dy	4.20	5.86	4.35	3.30	3.53	3.43	4.85	4.86	0.12
Er	1.32	1.40	2.03	0.99	1.25	1.19	1.64	2.26	0.10
Yb	-	-	-	0.78	0.81	0.87	1.07	1.85	0.05
Hf	9.51	6.88	8.23	6.93	6.59	-	8.31	-	-
Ta	-	0.40	-	0.30	0.39	-	0.97	-	-
Pb	13.8	9.61	19.1	13.9	14.8	15.1	13.6	1.89	0.04
Th	8.32	10.4	9.51	6.46	6.93	7.87	7.97	1.21	0.07
U	4.46	3.38	2.85	2.30	2.42	2.53	2.18	0.44	0.02

Notes: † Whole rock trace-element analysis performed by ICP-MS at Washington State University.
‡ V and Zn concentrations determined by XRF at Washington State University (Johnson et al., 1999).

DISCUSSION

Olivine-melt equilibria

The FeO*-MgO data collected from the naturally quenched inclusions from the scoria suggests that the liquidus temperature for the high forsterite olivine hosted inclusions is roughly 1100°C (based on a linear extrapolation of heating data; Fig. 3b). This temperature estimate is consistent with that predicted using COMAGMAT which suggests a liquidus temperature of 1115°C for the lava, using a water content of 5 wt% (estimated by difference) at 10 kbar (Ariskin et al., 1993). Using the temperature estimate of 1115ºC and the oxidation state of + 0.5 log units (ΔNNO) determined from the sulfur Kα peak shift, the $Fe^{3+}/\Sigma Fe$ of 0.25 can be calculated for the naturally quenched inclusions from scoria (following Sack et al., 1980).

Using the $Fe^{3+}/\Sigma Fe$ ratio of 0.25, $Kd_{ol\text{-}melt}$'s can be determined for the rehomogenized melt inclusions, naturally glassy inclusions, and the bulk lava compositions. A $Kd_{ol\text{-}melt}$ of 0.38 determined for the bulk lava suggests accumulation of 6.1% weight fraction of olivine, compared to a $Kd_{ol\text{-}melt}$ of 0.22 determined for the scoria, requiring that 4.9 wt% olivine be added back to the melt to be in equilibrium (assuming an equilibrium $Kd_{ol\text{-}melt}$ of 0.30; Roedder and Emslie, 1970). However, Kd's for the rehomogenized melt inclusions range from 0.07 to 0.62, and the low $Kd_{ol\text{-}melt}$ values associated with the high Fe contents suggests that these melts are not in equilibrium with the host olivines (Table 1). This finding is consistent with the increased FeO*/MgO of homogenized melt inclusions, as this produces melts that are further out of equilibrium

with olivine hosts. This evidence coupled with the lack of high FeO* concentrations in the host lava, the scoria, and naturally quenched inclusions, indicates that the high Fe concentrations observed in homogenized inclusions are not a primary feature of the originally trapped melt composition.

High Fe sources

The observed compositional changes in homogenized melts inclusions, together with petrologic evidence, suggest there are four potential sources for adding significant quantities of Fe into the silicate melt inclusions during rehomogenization; (i) the olivine host, and inclusions of (ii) chromite, (iii) sulfide or (iv) magnetite that are trapped together with the melt inclusion (if these were only daughter phases then reheating should simply add them back to the melt).

Addition of excess olivine, from heating of the inclusion above the temperature of trapping, could potentially introduce Fe into the inclusion. However, this should also dramatically increase the MgO concentration, which is high in Fo-rich olivine (Table 3). The trend expected for such addition is shown in Fig. 3. Although an increase in MgO is observed in the homogenized inclusions, the proportions of Fe to Mg cannot be explained by addition of Mg-rich olivine alone (Fig. 6). Likewise, although ubiquitous chromite inclusions would present another Fe source, Cr concentrations in homogenized inclusions are below detection limits (~500 ppm), whereas addition of sufficient chromite to explain the Fe increase (~55 wt% chromite) would produce a Cr content of 25 wt% Cr_2O_3. The observed increase in S with increasing FeO*, suggests that dissolution of a Fe-sulfide phase (either pyrite or pyrrhotite) is also a potential mechanism for Fe-gain. However,

Figure 4: Electron microprobe backscatter images of melt inclusions with oxides. (a) Coarse grained euhedral magnetite co-trapped with silicate glass in an unheated melt inclusion. (b) Coarse chromite grains trapped within a silicate melt inclusion next to an inclusion bearing a magnetite, rehomogenized at 1150°C. Increasing dissolution of magnetite grains into the silicate melt at (c) 1200°C and (d) 1225°C.

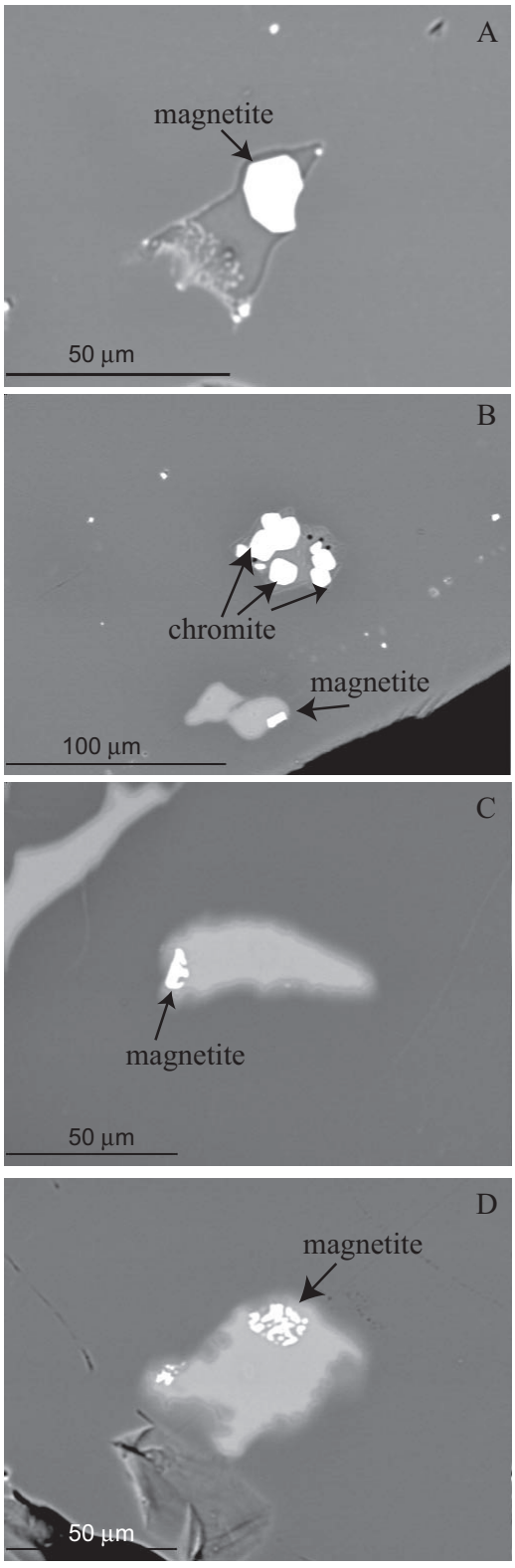
A
magnetite
50 µm
B
chromite
magnetite
100 µm
C
magnetite
50 µm
D
magnetite
50 µm

Figure 4.

both the increase in S and the S:FeO* in homogenized inclusions is far less (Fig. 3) than that required by addition of pyrite or pyrrhotite (with S:Fe weight ratios of ~1:1 and 1:2, respectively).

In light of the calculations above, the most likely source for the addition of Fe to the silicate melt is through the dissolution of a combination of magnetite + host olivine. Whereas in unheated inclusions magnetite grains are typically euhedral, as temperatures of rehomogenization are increased, dissolution of magnetite is evident in the increasingly wormy grain textures (Fig. 4). The average compositions of homogenized inclusions lie on a near linear trend (in Fe-Mg space), and a projection through the average values intersects a tie-line between olivine and magnetite at a ~1:1 atomic ratio (1:1.6 by weight; Fig. 6).

Magnetite formation

Despite the chemical and textural evidence for magnetite dissolution, there is still a question as to how the magnetite formed in the first place. Magnetite has previously been demonstrated to lie on or near the liquidus in H_2O-saturated conditions near the Ni-NiO oxygen buffer in calc-alkaline basalts and basaltic andesites (Sisson and Grove, 1993; Baker and Eggler, 1983). The addition of water under oxidizing conditions has the effect of destabilizing silicate minerals while not having a dramatic effect on oxides. The result is that magnetite, which commonly appears well below the liquidus after significant crystallization of silicates in dry magmas, crystallizes much closer to the liquidus, allowing it to co-exist with high forsterite olivine (Sisson and Grove, 1993). In addition, experimental work by Muan and Osborn (1956) in SiO_2-MgO-FeO•Fe_2O_3 systems has

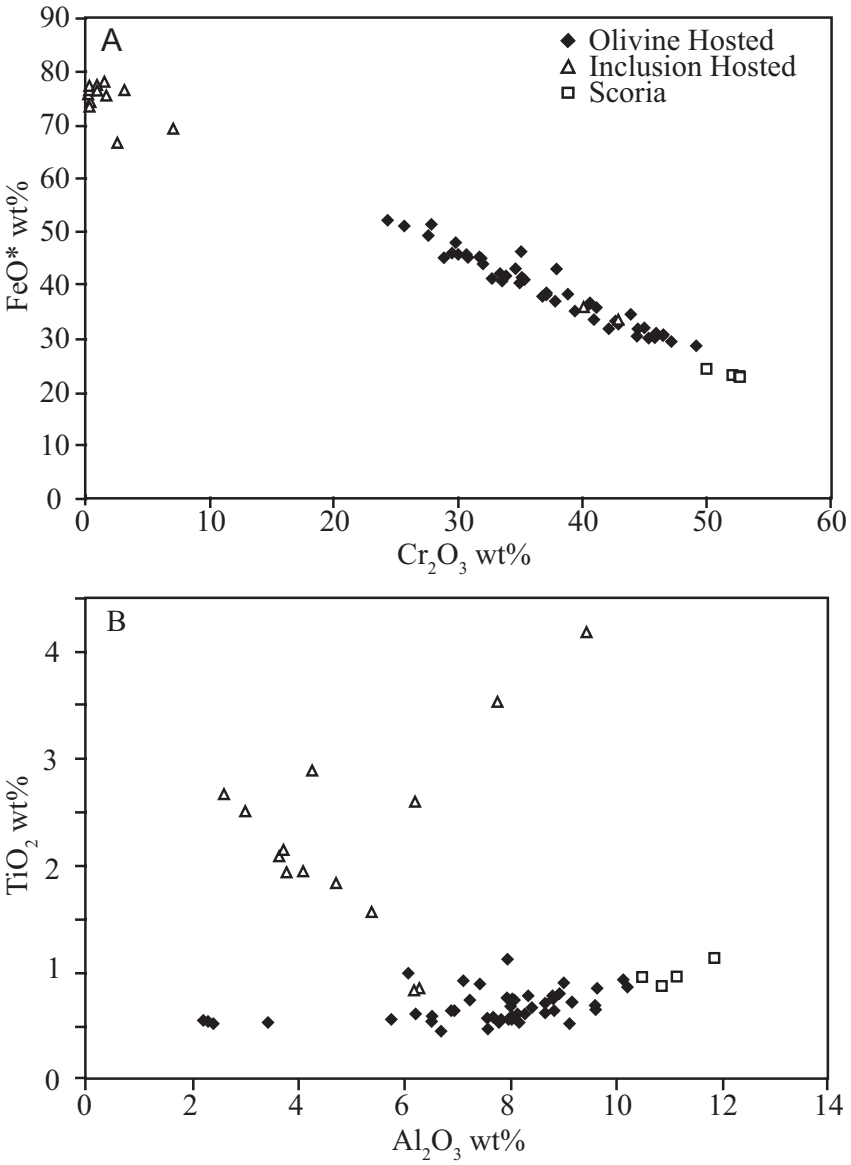

Figure 5: (a) TiO_2 versus Al_2O_3 and (b) FeO* versus Cr_2O_3 of spinels and magnetites from the lava and scoria samples. The lava sample is broken up into spinels trapped as mineral inclusions (solid diamonds) and spinels/magnetites trapped with melt (open triangles).

demonstrated that the cotectic between olivine, magnesiowustite and magnesioferrite migrates away from the MgO component as the system becomes more reduced (Fig. 7). The projection of the approximate 1:1.6 weight ratio onto the SiO_2-MgO-FeO•Fe_2O_3 ternary lies near the trend produced by the migration of the eutectic location (peritectic at lower fO_2). Importantly, if this model for magnetite formation is correct, it suggests that the olivine-magnetite ratio is not necessarily constant, but that it is case specific and dictated by the bulk composition and oxygen fugacity. Also, temperature does not seem to be a significant variable, at least for the restricted temperature range of this study, since little deviation is observed from the 1.6:1 weight ratio from 1125ºC to 1225ºC. However, if magnetite is a near-liquidus phase then it would also likely be co-trapped with melt inclusions in the scoria sample as well. As this is not the case, other methods for the formation of magnetite must also be considered.

Magnetite may also be forming in the melt inclusions post-entrapment. At high temperatures, H_2O dissociation may occur, allowing hydrogen to diffuse out of the melt inclusions. Hydrogen diffusion would result in excess oxygen, which may oxidize Fe^{2+} to Fe^{3+}. In order to maintain mineral-melt equilibrium, Fe^{2+} from the olivine would then be transferred to the melt. Assuming an unlimited supply of FeO, that all of the excess oxygen goes to converting FeO to Fe_2O_3, and that hydrogen does not significantly change phase equilibria (unlikely), then dissociation and diffusion of ~5 wt % H_2O from a trapped inclusion can produce 4.3 molar % magnetite with a residual melt composition up to 25 wt% FeO* prior to rehomogenization. In addition to the increasing Fe in the melt and magnetite crystallization, oxidation of the host olivine would also result in

Table 3: Representative spinel and olivine analyses.

Source	Scoria	Basalt Flow			Scoria	Basalt Flow
Mineral	Chromite	Magnetite	Magt-Chr_{SS}	Chromite	Olivine	Olivine
SiO_2	0.17	0.08	0.27	0.01	40.35	40.27
TiO_2	0.97	1.70	0.89	0.48	0.00	0.00
Al_2O_3	11.12	3.73	8.29	6.44	0.00	0.06
Cr_2O_3	52.06	1.26	31.77	45.17	0.03	0.05
FeO*	23.35	80.79	40.55	32.92	10.11	8.84
MnO	0.21	0.17	0.17	0.19	0.14	0.12
MgO	13.30	7.82	12.53	13.32	48.66	50.09
NiO	0.28	0.66	0.60	0.50	0.52	0.69
CaO	0.01	0.03	0.00	0.04	0.16	0.15
V_2O_5	0.04	0.00	0.04	0.01	-	-
ZnO	0.12	0.00	0.04	0.13	-	-
Total	101.63	96.24	95.15	99.21	99.97	100.26
Cations per formula unit (4 oxygen basis)						
Si	0.005	0.003	0.009	0.000	0.994	0.985
Ti	0.023	0.044	0.023	0.012	0.000	0.000
Al	0.413	0.152	0.329	0.248	0.000	0.002
Cr	1.302	0.035	0.848	1.170	0.001	0.001
Fe^{2+}	0.388	0.619	0.381	0.341	0.208	0.181
Fe^{3+}	0.227	1.719	0.759	0.557	-	-
Mn	0.006	0.005	0.005	0.005	0.003	0.002
Mg	0.625	0.404	0.628	0.648	1.786	1.826
Ni	0.007	0.018	0.016	0.013	0.010	0.014
Ca	0.000	0.001	0.000	0.001	0.004	0.004
V	0.001	0.000	0.001	0.000	-	-
Zn	0.003	0.000	0.001	0.003	-	-
Sum	3.000	3.000	3.000	3.000	3.006	3.014
$Fe^{2+}/Fe^{3+\dagger}$	1.70	0.36	0.50	0.61	-	-
Mg#	0.62	0.39	0.62	0.66	89.6	91.0
Cr#	0.76	0.19	0.72	0.83	-	-

Notes: *FeO as total iron.

† Fe^{2+}/Fe^{3+} determined after method of M. Clynne (personal communication).

Figure 6: (a) Atomic % Fe versus Mg for average melt inclusion compositions. Error bars are based on 1 standard deviation. Bold line represents a tie-line between olivine (ol) and magnetite (magt) compositions. Dashed arrow delineates increasing Fe and Mg trend with temperature, intersecting the tie-line at a 1:1 ratio. Thin line shows the addition of up to 30 wt% olivine to the melt (see text). (b) Enlargement of the dashed box from upper illustration (a).

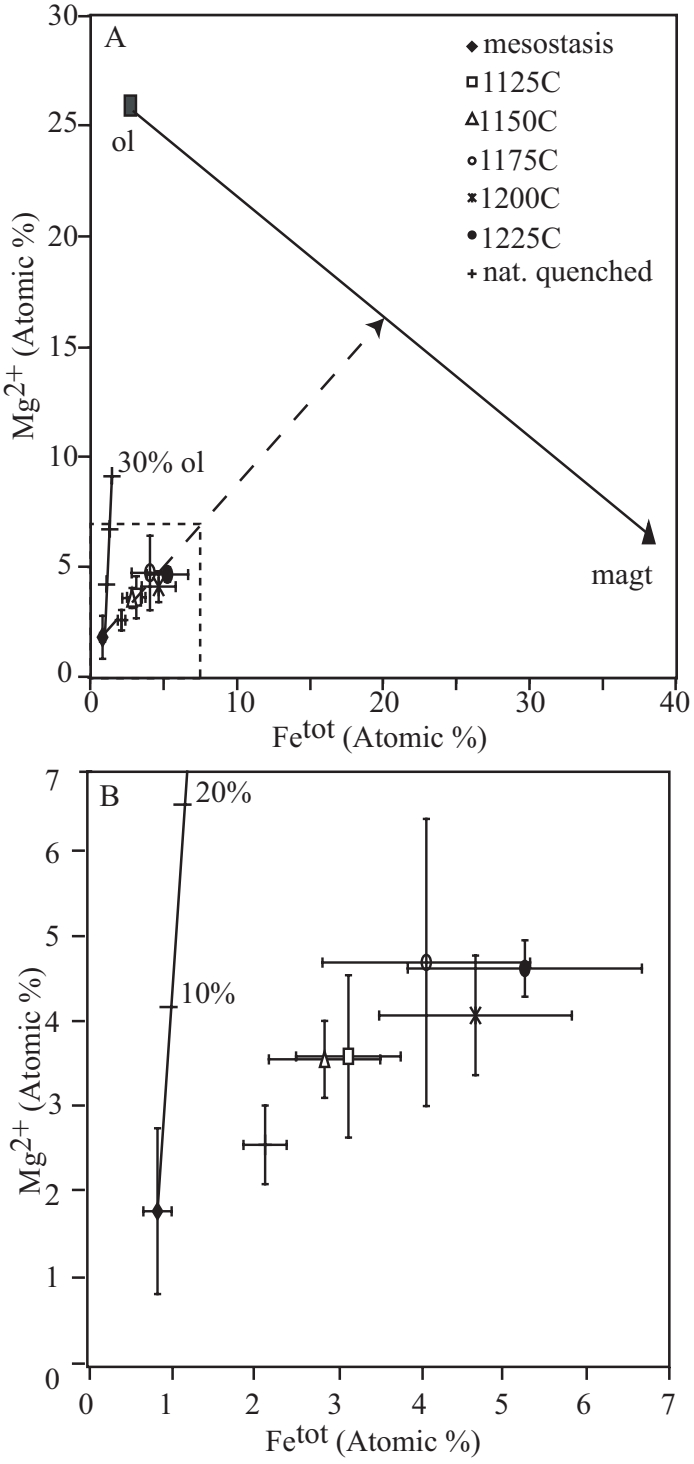
A
mesostasis
1125C
1150C
1175C
1200C
1225C
nat. quenched
ol
30% ol
magt
Mg^{2+} (Atomic %)
Fe^{tot} (Atomic %)
B
20%
10%
Mg^{2+} (Atomic %)
Fe^{tot} (Atomic %)

Figure 6.

crystallization of pyroxene, as is observed in many of the unheated melt inclusions (Lindsley, 1980). While this is an extreme case, it demonstrates that the high FeO* concentrations may be generated through hydrogen diffusion. However, as coarse grains of euhedral magnetite are present in the unheated inclusions prior to rehomogenization, their presence would imply that this process was occurring at high temperatures, likely while the olivines resided in the cooling lava. This model also supports the absence of magnetite from the scoria hosted melt inclusions which, due to rapid cooling have retained their high water concentrations, thus not allowing for Fe-pumping into the melt during hydrogen diffusion. Despite the cause of magnetite formation, it is clear that this process of Fe enrichment is a real phenomenon and not an artifact of the rehomogenization procedure.

MI rehomogenization

The most significant observations of this study are that magnetite dissolution during rehomogenization results in extremely high FeO* concentrations, and that the coarse magnetite grains must be formed at reasonably high temperatures either during transport or cooling in the lava flow. Applying these observations in an attempt to reconstruct the original trapped melt composition is then the next critical step. As described above, a common technique in melt inclusion studies is to incrementally add or subtract equilibrium olivine from the melt to account for host-mineral crystallization and to produce a composition in equilibrium with the host olivine (e.g. Danyushevsky et al., 2000; Sobolev and Chaussidon, 1996). However, gain of Fe significantly disturbs this calculation, as it alters the apparent Fe/Mg ratio of the melt. For example, for the

inclusions detailed herein, Fe-gain requires the incremental addition of up to 26.2 wt% equilibrium olivine to the melt to force the melt composition (1225°C average composition) into equilibrium with the host, creating melt compositions that differ from any observed natural lava, and more importantly, bear no resemblance to the magma from which the phenocryst grew (Table 4). Correct reconstruction of the original parent magma from the overheated melt inclusions requires subtraction of both olivine and magnetite from the melt. In the magnetite-olivine correction model outlined in Table 4, subtracting approximately 20% of a mixture of olivine and magnetite (1:1.6 wt%) from the 1225°C average composition will reconstruct a composition similar to the naturally quenched inclusions (Fig.2). Correcting that composition by addition of olivine to be in equilibrium with the host will then produce a composition more similar to the originally trapped magma. Comparing the results of this model to a reconstructed composition of a naturally quenched inclusion produces an excellent agreement for most major elements. The correction may become more complex when the formation of pyroxene, due to the oxidation of olivine, is also taken into account. However, due to the significantly greater proportion of Fe addition resulting from the melting of magnetite, the effects of the clinopyroxene crystallization are neglected in order to simplify recalculations.

Although we detail an example where Fe gain is large and readily detectable, smaller proportions of excess magnetite may be more difficult to detect, but may also alter FeO* contents and apparent melt-olivine equilibrium. If excess magnetite indeed forms as a result of H_2O dissociation and hydrogen diffusion, then high H_2O melts in which phenocrysts likely have maintained high temperatures for extended periods of time are

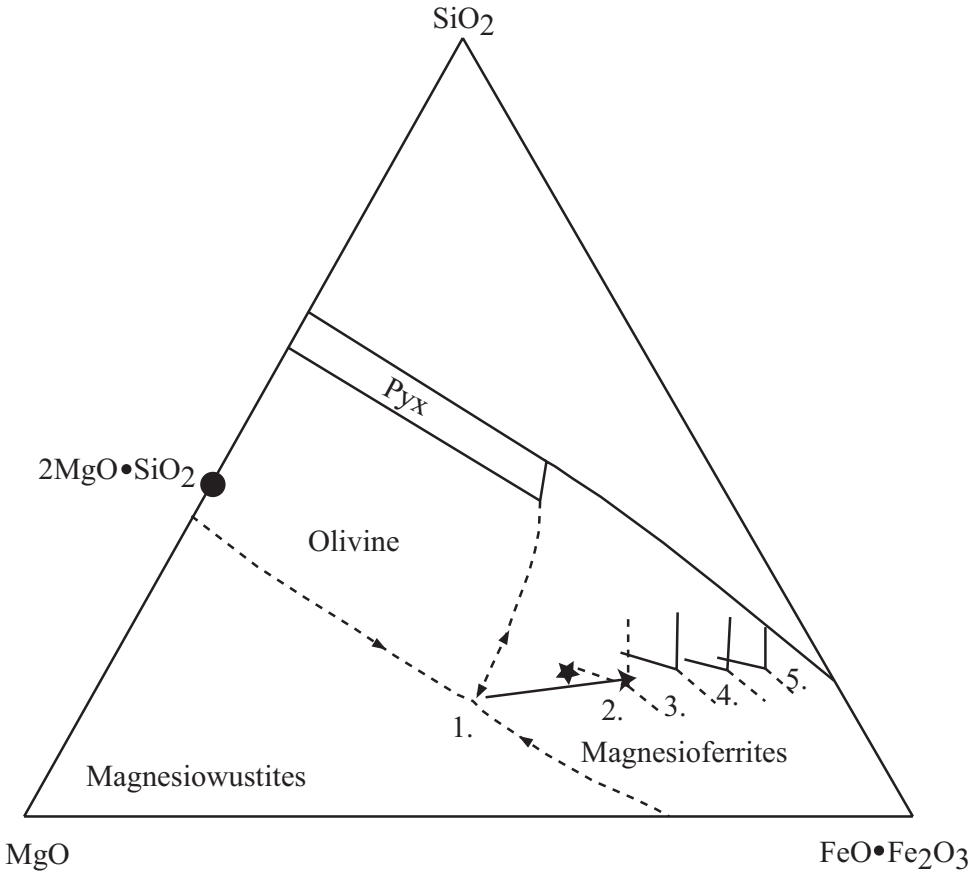

Figure 7: Ternary phase diagram for SiO_2-MgO-FeO•Fe_2O_3 (after Muan and Osborn, 1956). Location of eutectic (peritectic at points 2-5) at varying oxidation states determined from the experimental work of Muan and Osborn (1956). Experimental eutectic/peritectics are: 1) in air; 2) CO_2/H_2 =132; 3) CO_2/H_2 =40, 1440ºC, log fO_2 = -5.0; 4) CO_2/H_2 =24, 1410ºC, log fO_2 = -5.8; and 5) CO_2/H_2 =19, 1410ºC, log fO_2 = -6.0. The star represents the 1.6:1 (magnetite:forsterite) weight ratio determined from heating experiments. Note that the experimentally determined ratio intersects the trend produced by the migration of the eutectic/peritectic locations with decreasing oxidation state.

most at risk for experiencing Fe-gain. The most visible effects of the addition of the magnetite (dilution of silicate melt) are the low SiO_2 and Al_2O_3 and increased FeO* and FeO*/MgO (Fig. 2, 2). Modeling the effects of excess FeO* and MgO in the rehomogenized melt inclusions accurately reproduces the decreasing concentrations of the other major elements with increasing temperature (Table 1; Fig. 2c,d). In addition to the generally decreasing concentrations of other major elements with increased Fe dilution (increased temperature), there is also a large variability in melt inclusion composition for a given temperature. Much of this variability is due to the degree of dissolution of magnetite within individual inclusions at a constant temperature. Since the volumetric proportion of magnetite varies between different inclusions it is reasonable to conclude that the proportion of excess Fe, and thus the dilution of other major elements, will also vary between inclusions at a give temperature. This conclusion, unfortunately, restricts our ability to recalculate individual melt inclusion compositions, forcing us to rely on average compositions of suites of inclusions to correct for magnetite and olivine dissolution.

Cr, V, Ni, Co and Zn are known to substitute into magnetite and therefore produce anomalous trace metal contents in some instances (Deer et al., 1999). Additionally, experimental studies on magnetite-melt partitioning suggest that the high field strength elements (HFSE) Zr, Nb, Ta, and Hf are more compatible in Fe^{3+}-Ti rich spinels than in Cr-rich spinels, such that melting of magnetite into the silicate liquid should produce an anomalous increase in these components (Nielsen et al, 1994; Nielsen and Beard, 2000). However, in even the most extreme case (Table 4) only a 20% mixture, between 1:1.6

Table 4: Melt inclusion recalculations.

Sample	Naturally Quenched		1225°C Average Composition					
Process	Olivine Correction		Olivine Correction			Mt + Ol Correction		
Correction	Initial[†]	+ 9% Ol	Initial	+ 26.2% Ol	Dev.[#]	-20% Ol+Mt[‡]	+10.5% Ol	Dev.[#]
Na_2O	2.34	2.13	2.48	1.83	0.86	3.08	2.76	1.29
MgO	4.87	8.83	8.35	18.97	2.15	4.42	9.09	1.03
Al_2O_3	16.28	14.82	11.34	8.38	0.57	13.68	12.24	0.83
SiO_2	52.69	51.68	46.83	45.42	0.88	54.10	52.77	1.02
P_2O_5	1.31	1.20	1.07	0.82	0.68	1.33	1.20	1.00
S	0.44	0.40	0.54	0.40	1.01	0.68	0.61	1.52
Cl	0.16	0.15	0.10	0.07	0.50	0.12	0.11	0.76
K_2O	1.96	1.79	2.85	2.10	1.18	3.54	3.17	1.77
CaO	10.97	10.00	8.68	6.43	0.64	10.77	9.65	0.97
TiO_2	1.89	1.72	1.08	0.80	0.46	0.92	0.83	0.48
MnO	0.11	0.11	0.09	0.10	0.90	0.03	0.04	0.40
FeO*	5.22	5.59	13.00	12.03	2.15	5.34	5.76	1.03
Fe_2O_3*	1.91	1.73	3.86	2.85	1.64	2.39	2.14	1.23
Total	100.15	100.14	100.27	100.20		100.40	100.36	
$Kd_{ol\text{-}melt}$	0.20	0.30	0.12	0.30		0.16	0.30	

Notes: * FeO and Fe_2O_3 are determined after Sack et al. (1980).

[†]Initial naturally quenched composition is normalized on a water-free basis.

[‡]Mt+Ol ratio is 1:1.6 (wt%). Addition and subtraction of olivine (Ol) and magnetite (Mt) is in weight %.

[#]Deviation (Dev.) is the final corrected melt inclusion composition (K_D=0.3) divided by the corrected composition of the naturally quenched inclusion.

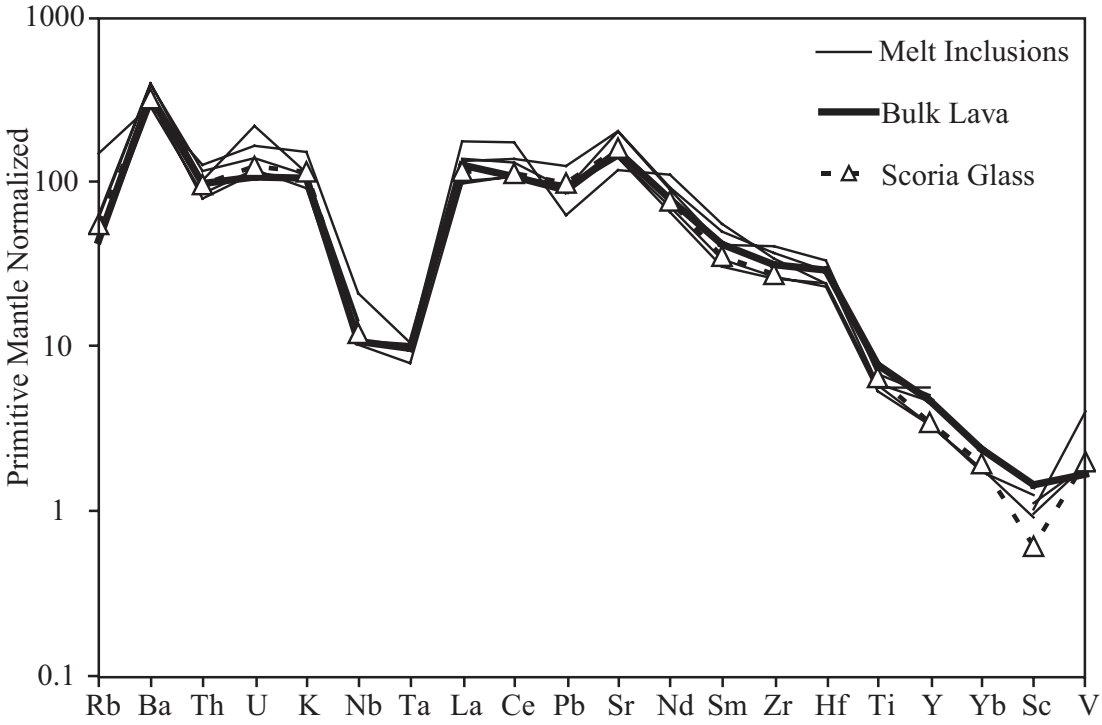

Figure 8: Primitive mantle normalized trace-element diagram. Trace elements are plotted for melt inclusions rehomogenized at 1200ºC (thin lines), lava (bold line), and average scoria composition (dashed bold line with triangles; see text; McDonough and Sun, 1995).

wt% ol-mt and melt, reconstructs the naturally quenched inclusion composition (Fig. 3). This recalculation equates to a ~12 wt% addition of magnetite to the silicate melt to produce the anomalous FeO* concentrations. While significant for major elements, an addition of 12 wt% magnetite to the melt does not produce an increase in trace element concentrations greater than the natural variability of the melt inclusion compositions (Fig. 8, Table 2).

Our heating experiments document a previously unreported phenomenon in melt inclusion rehomogenization studies. Simply correcting melt compositions to be in equilibrium with their host olivines by either adding or subtracting olivine is not a viable technique where significant quantities of magnetite are co-precipitating with olivine or forming through diffusion of hydrogen at high temperatures (Sisson and Grove, 1993). In such cases, the oxidation state, liquidus temperature of the melt, and water content need to be well constrained prior to rehomogenizing melt inclusions. Problems associated with excess Fe may therefore be particularly significant for magmas from subduction zone settings where oxidized and/or water-rich magmas are more common.

ACKNOWLEDGMENTS

The authors would like to thank Carl Thornber (Cascade Volcano Observatory) for his field assistance, and Ed Taylor and Anita Grunder (Oregon State University) for helpful comments and discussions. We would also like to thank John Donovan (University of Oregon) for his assistance with the S peak shift measurements. Reviews by D.

Kamenetsky, J Brophy, and M. Hirschmann helped to greatly improve this manuscript.

This work has been supported in part by a Kleinman Grant through the USGS.

REFERENCES

Ariskin, A., Frenkel M., Barmina, G., and Nielsen, R. (1993). COMAGMAT: A Fortran program to model magma differentiation processes. Computers and Geosciences, 19, 1155-1170.

Baker, D.R., and Eggler, D. (1983). Fractionation paths of Atka (Aleutians) high-alumina basalts: constraints from phase relations. Journal of Volcanology and Geothermal Research, 18, 387-404.

Carroll, M. and Rutherford, M. (1988). Sulfur speciation in hydrous experimental glasses of varying oxidation state: Results from measured wavelength shifts of sulfur X-rays. American Mineralogist, 73, 845-849.

Cervantes, P., and Wallace, P.J. (2003). The role of H_2O in subduction zone magmatism: New insights from melt inclusions in high-Mg basalts from Central Mexico. Geology, 31, 235-238.

Conrey, R., Sherrod, D., Hooper, P., and Swanson, D. (1997). Diverse primitive magmas in the Cascade arc, Northern Oregon and Southern Washington. The Canadian Mineralogist, 35, 367-396.

Danyushevsky, L. V., Della-Pasqua, F.N., and Sokolov, S. (2000). Re-equilibration of melt inclusions trapped by magnesian olivine phenocrysts from subduction-related magmas: petrological implications. Contributions to Mineralogy and Petrology, 138, 68-83.

Danyushevsky, L. V., McNeill, A.W., and Sobolev, A. (2002). Experimental and petrological studies of melt inclusions in phenocrysts from mantle-derived magmas: an overview of techniques, advantages and complications. Chemical Geology, 183, 5-24.

Deer, W.A., Howie, R., and Zussman, J. (1999). An introduction to the rock-forming minerals (2^{nd} edition). 696 p., Pearson Education Limited, Essex, England.

Gaetani, G. A. and Watson, E.B. (2000). Open-system behavior of olivine-hosted melt inclusions. Earth and Planetary Sciences, 183, 27-41.

Hauri, E. H. (2002). SIMS analysis of volatiles in silicate glasses, 2: isotopes and abundances in Hawaiian melt inclusions. Chemical Geology, 183, 115-141.

Johnson, D.M., Hooper, P.R., and Conrey, R. M. (1999). XRF analysis of rocks and minerals for major and trace elements on a single low dilution Li-tetraborate fused bead. Advances in X-ray Analysis, 41, 843-867.

Katsura, T., and Muan, A. (1964). Experimental study of equilibria in the system FeO-Fe_2O_3-Cr_2O_3 at 1300ºC. Transactions of the American Institute of Mining and Metallurgical Engineers, 230, 77-84.

Kamenetsky, V. S., Crawford, A.J., Eggins, S.M., and Muehe, R. (1997). Phenocryst and melt inclusion chemistry of near-axis seamounts, Valu Fa Ridge, Lau Basin: insight into mantle wedge melting and the addition of subduction components. Earth and Planetary Science Letters**,** 151, 205-223.

Kamenetsky, V.S., Crawford, A.J., and Meffre, S. (2001). Factors controlling chemistry of magmatic spinel: an empirical study of associated olivine, Cr-spinel and melt inclusions from primitive rocks. Journal of Petrology, 42, 655-671.

Kent, A.J.R., and Elliot, T.R. (2002). Melt inclusions from Mariana arc lavas: Implications for the composition and formation of island arc magmas. Chemical Geology, 183, 265-288.

Kent, A.J.R., Baker, J.A., and Wiedenbeck, M. (2002). A melt inclusion-based study of crustal contamination and melt column aggregation in continental flood basalts from Yemen. Earth and Planetary Science Letters, 202, 577-594.

Kent, A.J.R., Stolper, E.M., Francis, D., Woodhead, J., Frei, R. and Eiler, J. (2004). Mantle heterogeneity during the formation of the North Atlantic Tertiary Province: Constraints from trace element and Sr-Nd-Os-O isotope systematics of Baffin Island picrites. Geochemistry, Geophysics, Geosystems, 5, Q11004, doi:10.1029/2004GC000743.

Lindsley, D. (1976). Experimental studies of oxide minerals. In Oxide Minerals, Mineralogical Society of America Short Course Notes, 3, L61-L88.

Lindsley, D. (1980). Phase equilibria of pyroxenes at pressures >1 atmosphere. In Pyroxenes, Reviews in Mineralogy, 7, 289-307.

McDonough, W.F., and Sun, S-s. (1995). The composition of the Earth. Chemical Geology, 120, 223-253.

Muan, A., and Osborn, E. (1956). Phase equilibria at liquidus temperatures in the system MgO-FeO-Fe_2O_3-SiO_2. Journal of the American Ceramic Society, 39, 121-140.

Nielsen, R. L. and Beard, J. (2000). Magnetite-melt HFSE partitioning. Chemical Geology, 164, 21-34.

Nielsen, R.L., Forsythe, L., Gallahan, W., and Fisk, M. (1994). Major- and trace-element magnetite-melt equilibria. Chemical Geology, 117, 167-191.

Nielsen, R. L., Crum, J., Bourgeois, R, Hascall, K., Forsythe, L, Fisk, M., and Christie, D. (1995). Melt inclusions in high-An plagioclase from the Gorda Ridge: an example of the local diversity of MORB parent magmas. Contributions to Mineralogy and Petrology, 122, 34-50.

Nielsen, R.L., P. Michael, and Sours-Page, R. (1998). Chemical and physical indicators of compromised melt inclusions. Geochimica et Cosmochimica Acta, 62, 831-839.

Qin, Z., Lu, F., and Anderson, A. (1992). Diffusive re-equilibration of melt and fluid inclusions. American Mineralogist, 77, 565-576.

Roedder, E. and Emslie, R. (1970). Olivine-liquid equilibrium. Contributions to Mineralogy and Petrology, 29, 275-289.

Saal, A.E., Hart, S.R., Shimizu, N., Hauri, E.H., and Layne, G.D. (1998). Pb isotopic variability in melt inclusions from ocean island basalts, Polynesia. Science, 282, 1481-1484.

Sack, R., Carmichael, I., Rivers, M., and Ghiroso, M. (1980). Ferric-ferrous equilibria in natural silicate liquids at 1 bar. Contributions to Mineralogy and Petrology, 75, 369-376.

Sisson, T. W. and Bronto, S. (1998). Evidence for pressure-release melting beneath magmatic arcs from basalt at Galunggung, Indonesia. Nature, 391, 883-886.

Sisson, T., and Grove, T. (1993). Experimental investigations of the role of H_2O in calc-alkaline differentiation and subduction zone magmatism. Contributions to Mineralogy and Petrology, 113, 143-166.

Sisson, T. W. and Layne, G. D. (1993). H_2O in basaltic and basaltic andesite glass inclusions from four subduction-related volcanoes. Earth and Planetary Science Letters 117, 619-637.

Sobolev, A. V. and Chaussidon, M. (1996). H_2O concentrations in primary melts from suprasubduction zones and mid-ocean ridges: Implications for H_2O storage and recycling in the mantle. Earth and Planetary Science Letters, 137, 45-55.